JACC: BASIC TO TRANSLATIONAL SCIENCE VOL. 5, NO. 11, 2020

PRECLINICAL RESEARCH

Transcatheter-Delivered Expandable Bioresorbable Polymeric Graft With Stenting Capacity Induces Vascular Regeneration

Renee Duijvelshoff, MD, PhD,[a,b,*] Maria S. Cabrera, PhD,[c,*] Bart Sanders, PhD,[c,*] Sylvia Dekker, MSc,[a] Anthal I.P.M. Smits, PhD,[a,b] Frank P.T. Baaijens, PhD,[a,b] Carlijn V.C. Bouten, PhD[a,b]

VISUAL ABSTRACT

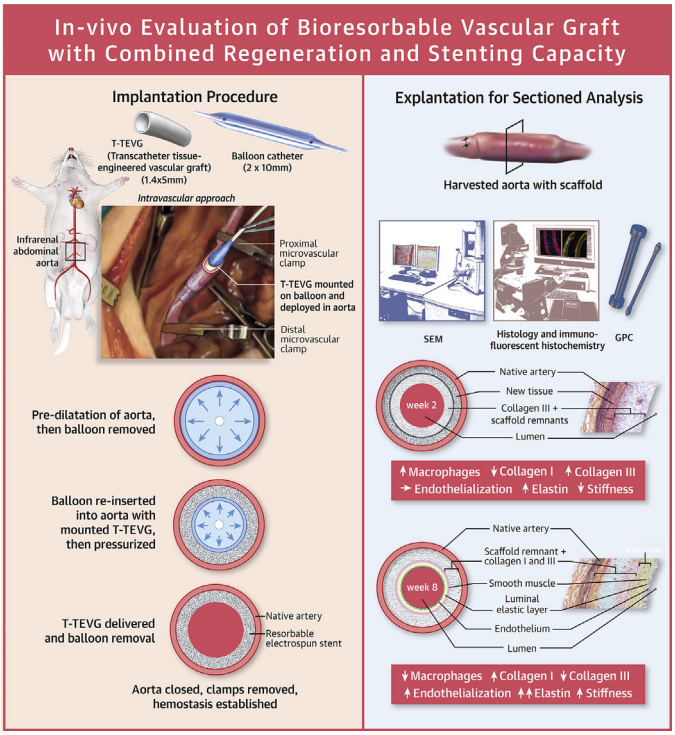

Duijvelshoff, R. et al. J Am Coll Cardiol Basic Trans Science. 2020;5(11):1095–110.

HIGHLIGHTS

- **We designed a transcatheter balloon-expandable resorbable vascular graft with support capacity.**
- **After 2 months in vivo, grafts show native-like tissue reconstruction with endoluminal elastin.**
- **The concept convenes regenerative grafting, minimally invasive delivery, and clinical stenting.**

From the [a]Department of Biomedical Engineering, Eindhoven University of Technology, Eindhoven, the Netherlands; [b]Institute for Complex Molecular Systems, Eindhoven, the Netherlands; and [c]Stentit B.V., Eindhoven, the Netherlands. *Drs. Duijvelshoff, Cabrera, and Sanders contributed equally to this work and are joint first authors.

The authors attest they are in compliance with human studies committees and animal welfare regulations of the authors' institutions and Food and Drug Administration guidelines, including patient consent where appropriate. For more information, visit the *JACC: Basic to Translational Science* author instructions page.

Manuscript received May 11, 2020; revised manuscript received September 14, 2020, accepted September 14, 2020.

ISSN 2452-302X https://doi.org/10.1016/j.jacbts.2020.09.005

JACC: BASIC TO TRANSLATIONAL SCIENCE VOL. 5, NO. 11, 2020
NOVEMBER 2020:1095–110

ABBREVIATIONS AND ACRONYMS

BVS = bioresorbable vascular scaffold(s)

ECM = extracellular matrix

GPC = gel permeation chromatography

M_w = weight-average molecular weight

PBS = phosphate-buffered saline

SEM = scanning electron microscopy

SMA = smooth muscle actin

SMC = smooth muscle cell

TE = tissue engineering

T-TEVG = transcatheter tissue-engineered vascular graft

SUMMARY

As the next step in the translation of vascular tissue engineering, this study uniquely combines transcatheter delivery and in situ tissue regeneration using a novel bioresorbable electrospun polymer graft that can be implanted minimally invasively. Once delivered inside a small-diameter vessel, the electrospun microstructure supports the vessel wall, facilitates cellular infiltration, and guides organized tissue formation.

There is an immense clinical demand for small-diameter vascular replacements (e.g., for coronary or peripheral artery diseases as well as arteriovenous shunts or congenital malformations). The gold standard for small-diameter arterial replacement remains the patient's own artery or vein (e.g., internal thoracic artery, radial artery, great saphenous vein), because of its superior biocompatibility and long-term patency (1–3). However, autologous vessels are not always available for grafting, because of vascular disease, previous harvest, or when multiple or lengthy bypasses are required (4,5). In addition, it requires additional surgery, with risk for harvest-site morbidity (5).

To date, synthetic vascular alternatives are mainly made of nondegradable surgical polytetrafluoroethylene grafts, which have proved to be successful in the replacement of large-diameter arteries (≥6 mm) (1). However, when small-diameter vascular conduits are required (≤6 mm), polytetrafluoroethylene grafts exhibit poor patency rates compared with autologous vessels (1,6,7). This has been attributed to surface thrombogenicity of the conduits, the absence of an endothelial layer, and anastomotic intimal hyperplasia, which results from hemodynamic disturbances due to a mismatch in compliance between the elastic native artery and the relatively rigid prosthesis (8).

To address the lack of suitable small-diameter vascular conduits, many vascular tissue engineering (TE) strategies have been explored, ranging from in vitro engineering of vessels in the laboratory to in situ engineering of vessels inside the human body (9–18). The latter relies on the notion that endogenous regeneration can be induced directly at the implantation site by harnessing the regenerative potential of the human body using instructive biodegradable surgical grafts (19). Recently, this in situ TE approach has gained increasing attention because it offers off-the-shelf availability and is cost-effective (20). In addition, these biodegradable grafts are tailorable not only by material choice and processing but also through graft structural design. In this way, off-the-shelf grafts could transform into native-like arteries to improve long-term functionality (1,6,7). Unfortunately, placement of these promising regenerative conduits thus far has always required open surgery, and many mechanical failures such as aneurysmal dilatations have been observed (21).

As a next step in the transition to a less invasive interventional approach, we developed a vascular graft suitable for transcatheter delivery, because of its capacity to expand and exert forces onto existing vessels, and can induce vascular regeneration because of its bioresorbable electrospun structure. Although other expandable and resorbable scaffolds have been and are currently under investigation, their slotted tubular structures are favorable to expand and provide temporary support to the artery but limit their capacity of tissue regeneration (22–30). The technology we present, in contrast, is distinguished by relying on an electrospun fibrous microarchitecture, which we hypothesize to be key in achieving a favorable microenvironment to induce in situ tissue regeneration, on the basis of previous findings with electrospun engineered vascular interposition grafts (31,32). To that end, we combined the use of a biodegradable material with a microfibrous structural graft design that allows transcatheter delivery and exerts sufficient force to instantly secure itself into the vascular wall upon deployment, while providing a template for colonizing cells to induce neotissue formation (Supplemental Figure S1).

The objectives of this proof-of-concept study were to successfully deliver transcatheter tissue-engineered vascular grafts (T-TEVGs) in a minimally invasive approach and to assess their regenerative potential by means of cellular infiltration and the onset of early tissue production, in relation to patency. T-TEVGs were delivered minimally invasively into the abdominal aortas of rats using a balloon catheter and explanted at pre-determined time points over the course of 8 weeks. Explants

were characterized for patency, extracellular matrix (ECM) composition, cellularization, mechanical properties, and degradation using histology, immunohistochemistry, scanning electron microscopy (SEM), mechanical testing, and gel permeation chromatography (GPC).

METHODS

STUDY OBJECTIVE. The aim of this study was to evaluate the in vivo potential and performance of a novel regenerative vascular graft for revascularization in a small animal model. The objectives of this proof-of-concept study were to "explore" a minimally invasive approach to safely deliver and deploy the vascular graft and to evaluate regenerative potential. This study received the proper ethical oversight.

T-TEVG FABRICATION. For this study, novel T-TEVGs (n = 20) were used (Stentit B.V., Eindhoven, the Netherlands). On a 1.4-mm mandrel, poly-L-lactic acid-based biomaterial (Corbion Purac, Gorinchem, the Netherlands) was processed into fibrous tubular conduits using conventional electrospinning technology, inside a climate-controlled electrospinning cabinet (IME Medical Electrospinning, Geldrop, the Netherlands). The resulting tube diameter, wall thickness, and averaged fiber diameter were evaluated using SEM (Quanta 600F, FEI, Hillsboro, Oregon). Prior to implantation, tubes were cut to size and sterilized using gradient alcohol series. Control samples (n = 9) were characterized upon inflation on maintained luminal area, wall thickness, and fiber morphology using SEM in combination with standard image-processing software (ImageJ version 1.52, National Institutes of Health, Bethesda, Maryland).

ANIMAL STUDIES. In vivo functionality of the regenerative T-TEVG was studied during short-term follow-up in a rat model. Following a successful in vivo experiment of 24-h follow-up (n = 1), we monitored delivery, patency, neotissue formation, cellular infiltration, endothelialization, T-TEVG resorption, and mechanical properties of T-TEVGs up to 2 (n = 4), 4 (n = 4), 6 (n = 4), and 8 (n = 4) weeks of follow-up.

All of the animal experiments were reviewed and approved by the Animal Ethics Committee of Maastricht University and conformed to the guidelines for the use of laboratory animals, as formulated by Dutch law on animal experimentation. Twenty inbred male Lewis rats (Charles River Laboratories, Sulzfeld, Germany) weighing 389 ± 35 g were used in this study. Animals were housed in pairs in individually ventilated cages at 20°C and 50% humidity on a 12-h light-dark cycle with ad libitum access to standard chow and water. After 1 week of acclimatization, animals were enrolled in the study and underwent T-TEVG placement into the abdominal aorta. T-TEVGs were explanted after 1 day (n = 1), 2 weeks (n = 4), 4 weeks (n = 4), 6 weeks (n = 4), and 8 weeks (n = 4). In addition, part of the native abdominal aorta of each animal was explanted.

IMPLANTATION PROCEDURE. Prior to surgery, animals were given subcutaneous analgesia (buprenorphine 0.05 mg/kg).

T-TEVG implantations were performed under general anesthesia (1.5% to 2.5% isoflurane) and under sterile conditions in spontaneously breathing animals under microscopic view (Leica Microsystems, Wetzlar, Germany). Body temperature was maintained at 37°C using a heating pad. After a midline laparotomy, the aorta was prepared from the surrounding tissues from the level of the renal arteries down to the bifurcation. Microvascular clamps were placed to stop aortic blood flow. A small transverse incision was made, approximately 2 to 3 mm below the proximal microvascular clamp, to open the aorta, which was subsequently flushed with heparin (150 to 200 U). A 2-mm balloon catheter (NuMed Mini Ghost, Heart Medical Europe, Best, the Netherlands) was inserted and inflated to 14 atm for 60 s to pre-dilate the aorta and facilitate insertion of the T-TEVG. The T-TEVGs (1.4 × 5 mm) were mounted on the balloon catheter, which was pre-pressurized to 0.5 atm for T-TEVG fixation. After delivery of the T-TEVGs to the desired location, pressurization at 14 atm enabled T-TEVG deployment. After deflation and removal of the balloon catheter, the incision was closed by interrupted 8-0 nylon sutures (Ethilon, Ethicon End-Surgery, Johnson and Johnson, New Brunswick, New Jersey). When the clamps were removed and hemostasis was achieved, the aorta was closely inspected to confirm pulsatile flow distal to the T-TEVG. The abdomen was closed in 2 layers using 4-0 sutures (Vicryl, Ethicon Endo-Surgery, Johnson and Johnson). Animals recovered in a chamber at 30°C and were assessed for body weight changes and signs of thrombosis (paralysis of lower extremities). At the end of the day of surgery, animals were given subcutaneous analgesia (buprenorphine 0.05 mg/kg). During the first 7 post-operative days, animals were given subcutaneous analgesia (carprofen 4 mg/kg) once a day. No other medication was given throughout the duration of the study.

EXPLANTATION PROCEDURE. Animals were sacrificed at pre-determined time points of 1 day (n = 1), 2 weeks (n = 4), 4 weeks (n = 4), 6 weeks (n = 4), and 8 weeks (n = 4). Animals were euthanized under

isoflurane anesthesia by exsanguination and systematically perfused with cold phosphate-buffered saline (PBS) (Sigma-Aldrich, St. Louis, Missouri). The aorta was carefully harvested, and segments of the proximal, distal, and scaffolded aorta were collected for further cutting. Specimens for histology and immunohistochemistry were fixated in 3.7% formalin for 24 h at 4°C. Cross sections were prepared by embedding the tissue in paraffin and cutting sections 5 μm thick. Deparaffinization was performed in xylene and dehydration in a graded series of ethanol. Specimens for SEM were fixated in 2.5% glutaraldehyde for 24 h at 4°C and dehydrated in a graded ethanol series, starting from 50% to 100% in 5% to 10% increments, after which the ethanol was allowed to evaporate.

EXPLANT HISTOLOGY. Following dehydration, the specimens were stained with Weigert's hematoxylin and eosin (Sigma-Aldrich), Russell-Movat Pentachrome (American MasterTech, Lodi, California), and Elastica von Gieson (Merck, Darmstadt, Germany) to assess gross morphology and tissue composition. Alizarin Red S (Sigma-Aldrich) and von Kossa (33) stains were performed to assess calcium deposits. Stained slides were dehydrated through either acetone and acetone-xylene (1:1) (Alizarin Red) or graded alcohol (von Kossa), cleared in xylene, and subsequently mounted in Entellan (Merck). Tile scans and pictures were recorded using a Zeiss Axio 681 Observer Z1 microscope (Carl Zeiss Microscopy, Jena, Germany). Luminal area was measured from histological images using standard image-processing software (ImageJ version 1.52).

EXPLANT IMMUNOHISTOCHEMISTRY. Following rehydration, different antigen retrievals were performed depending on the primary antibody used (Supplemental Table S1), heat-mediated in a 96°C water bath for 20 min in citrate buffer (pH 6.1; DAKO) or Tris/EDTA buffer (pH 8; Sigma). The buffer was then allowed to cool, after which slides were washed. This was followed by a permeabilization step with 0.5% Triton-X-100 (Merck) in PBS for 10 min at room temperature. For enzymatic antigen retrieval, 0.05% pepsin (Sigma-Aldrich) in 10 mmol/l HCl was applied to the tissue slides for 12 min at 37°C. Blocking was performed by incubating slides in 1% nonfat dry milk, 1% bovine serum albumin, 2% normal goat serum (Invitrogen, Carlsbad, California), and 0.3 mol/l Glycin (Sigma-Aldrich) in 0.05% Tween-20 (Merck) in PBS for 1.5 h at room temperature. Primary antibodies (Supplemental Table S1) were prepared at the desired concentrations in 1:10 diluted blocking buffer and were applied overnight at 4°C. All washing steps were done with 0.05% Tween-20 in PBS. The following day, slides were washed and incubated with their secondary antibody. All primary antibodies, with the exception of CD31, were incubated with Alexa Fluor 488/555/647 secondary antibodies (1:500; Molecular Probes, Thermo Fisher Scientific, Waltham, Massachusetts) for 1.5 h at room temperature. Cell nuclei were stained with 4′,6-diamidino-2-phenylindole (DAPI). Stained slides were mounted in Mowiol (Calbiochem, San Diego, California). The CD31 primary antibody was incubated with a biotin-labelled secondary antibody (1:500; Vector BA-1000, Vector Laboratories Inc, Burlingame, California), and to enhance staining, an ABC-alkaline phosphatase kit (VECTASTAIN ABC-AP Staining kit, Vector Laboratories Inc.) was used for one hour at room temperature, according to the manufacturer's guidelines. After washing, the slides were exposed to a SIGMA FASTtm BCIP/NBT (Bromo-4-chloro-3indolyl phosphate/Nitro blue tetrazolium; Sigma). Stained slides were mounted in Entellan (Merck, Darmstadt, Germany). Incubation with secondary antibody only was included as a negative control. Tile scans and pictures were recorded with either a Zeiss Axio 681 Observer Z1 microscope (Carl Zeiss Microscopy) or a Zeiss Axiovert fluorescence microscope (Carl Zeiss Microscopy).

QUANTITATIVE IMMUNOHISTOCHEMICAL ANALYSIS. Cellularity was studied using DAPI staining. For each time point (weeks 2, 4, 6, and 8), 3 explants were analyzed. For each explant, 4 random areas were selected and digitally photographed using a Zeiss Axiovert fluorescence microscope. These images were converted into 8-bit grayscale images and further analyzed using ImageJ. After selecting, duplicating, and measuring the area of interest, a threshold was set. Cell nuclei were separated by water shedding and subsequently counted using ImageJ. Cell number was adjusted to measured area to allow an equal comparison of the 4 images. The mean of the 3 images was then calculated.

Quantification of CD68 and alpha-smooth muscle actin (α-SMA) was studied using immunostaining of each marker. For each time point (weeks 2, 4, 6, and 8), 3 explants were analyzed. For each explant, 4 random areas were selected and digitally photographed using a Zeiss Axiovert fluorescence microscope. These images were converted into 8-bit grayscale images and further analyzed using ImageJ. After selecting and duplicating the area of interest, a threshold was set. The area fraction of each marker was measured using ImageJ. The mean of the 4 images was then calculated.

FIGURE 1 T-TEVG Appearance Pre-Implantation, During Implantation, and After Explantation

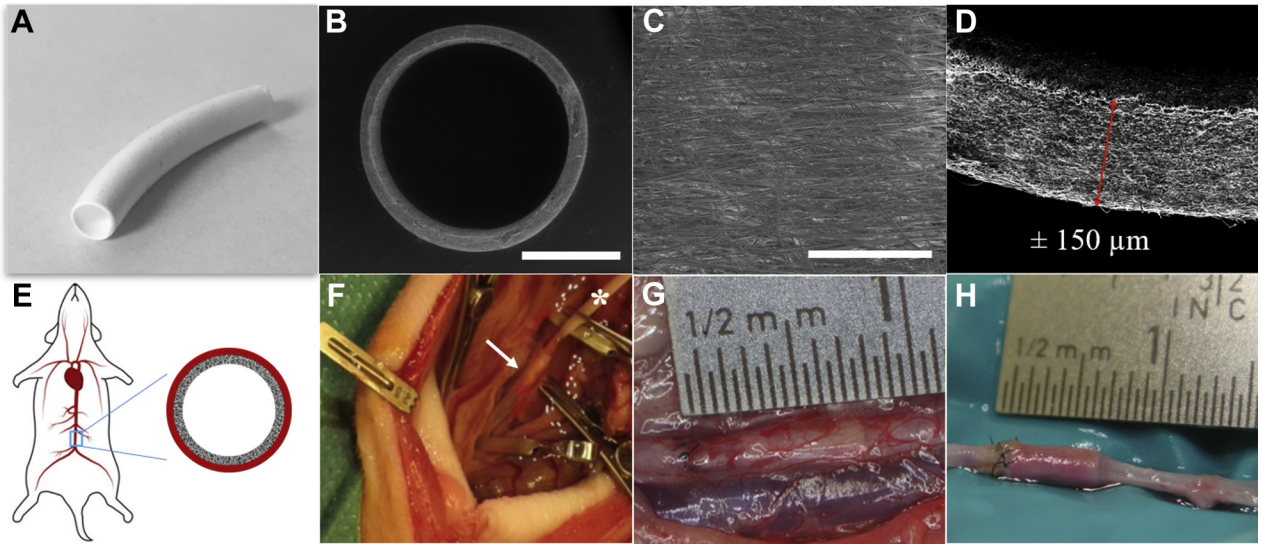

(A) Transcatheter tissue-engineered vascular graft (T-TEVG) pre-implantation. **(B)** Scanning electron microscopic (SEM) image of T-TEVG pre-implantation (cross section). Scale bar represents 1 mm. **(C)** SEM image of T-TEVG pre-implantation (luminal view). Scale bar represents 100 μm. **(D)** SEM image of T-TEVG pre-implantation (wall thickness). **(E)** Schematic view of implantation site (infrarenal abdominal aorta). **(F)** Surgical view of T-TEVG **(arrow)** delivery using a balloon catheter **(asterisk)**. Head of the animal situated above picture. **(G)** Surgical view of T-TEVG in situ. Head of the animal situated left from picture. **(H)** T-TEVG within the native aorta after explantation.

EXPLANT EVALUATION BY SEM. Explants were dehydrated using gradual increasing alcohol series and evaporated in a vacuum chamber overnight. Samples were analyzed using SEM (Quanta 600F) under low vacuum, with an electron beam of 7 kV to visualize the morphology of the T-TEVG, neotissue formation, and endothelialization. Graft-specific SEM measurements were made using internal machine software (Quanta 600F).

EXPLANT MECHANICAL PROPERTIES. Ring specimens from the native aorta, the bare graft, and the grafted aorta were obtained for uniaxial ring tensile testing (34). Tissue samples were snap frozen and stored at −80°C until use. After thawing, the thickness of the samples (t_0) was determined from scanning electron microscopic images, using an average of 6 measurements for stress calculations. The width of the samples (w_0) was determined from microscopic images, using an average of 3 measurements for stress calculations (Supplemental Figure S2). Force-displacement curves were obtained from uniaxial tensile tests (CellScale, Waterloo, Ontario, Canada). The samples were mounted as indicated in Supplemental Figure S2 and tested until break at a constant speed of 0.027 mm/s. Testing was performed at 37°C in a PBS bath.

Engineering stresses (σ) and engineering strains (ε) were calculated according to equations 1 and 2, respectively. The force (F) and length were determined from tensile tests, where the initial length (l_0) and the final length (l_f) represent the distance between clamps before and after stretching the sample (Supplemental Figure S2). The secant moduli were calculated from the stress and strain curves according to equation 3, where a low-strain modulus ($S1$) and a high-strain modulus ($S2$) was determined.

$$\sigma = \frac{F}{2A_0} = \frac{F}{2t_0 w_0} \quad (1)$$

$$\varepsilon = \frac{l_f - l_0}{l_0} \quad (2)$$

$$S = \frac{\sigma_2 - \sigma_1}{\varepsilon_2 - \varepsilon_1} \quad (3)$$

EXPLANT ANALYSIS BY GPC. The effect of hydrolysis on the molecular weight of the polymer was assessed using GPC. The GPC measurements (n = 17) were performed on a Mixed-D column (300 × 7.5 inside diameter, 5lm particles, Agilent Technologies, Santa Clara, California) using chloroform at 1 ml/min as the mobile phase and a photodiode array

FIGURE 2 Gross Morphology of T-TEVGs After Explantation

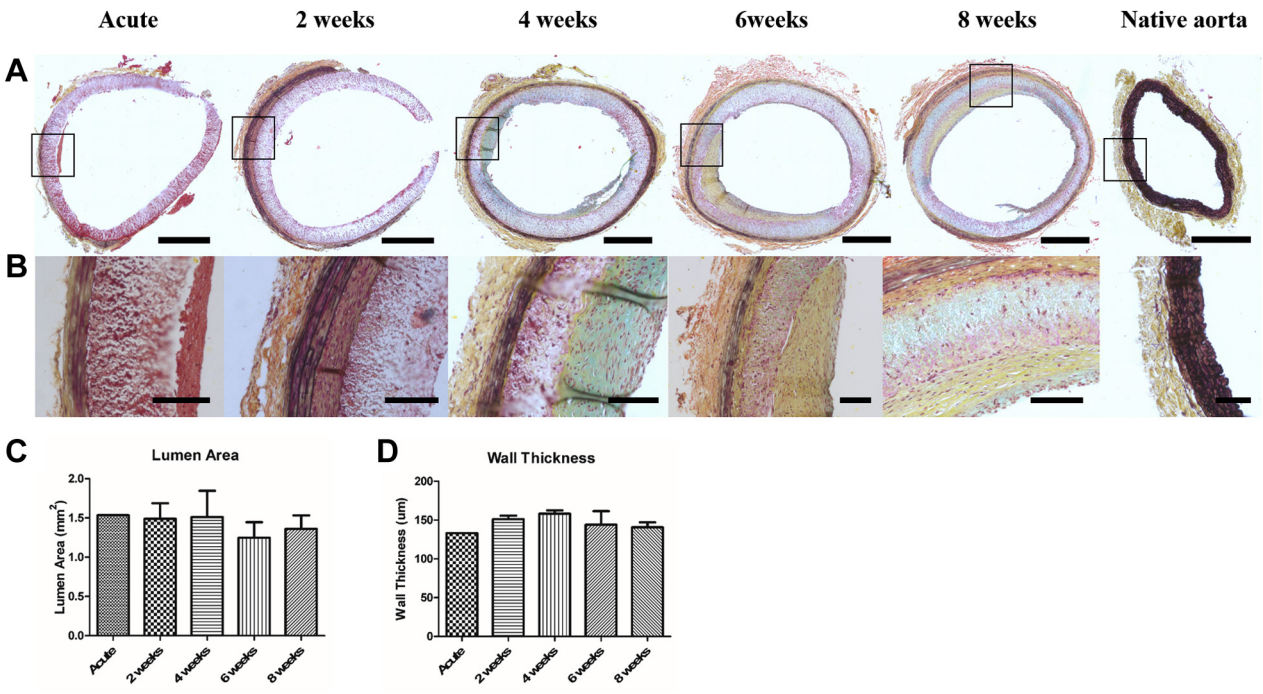

(A,B) Russell-Movat Pentachrome staining of midgraft transcatheter tissue-engineered vascular graft (T-TEVG) and native rat aorta. Scale bars represent 500 μm **(A)** and 100 μm **(B)**. **(C)** Luminal area (± SD) of T-TEVGs measured from histological images in square millimeters. **(D)** Wall thickness (± SD) of T-TEVGs measured from histological images in micrometers.

(SPD-M20A, Shimadzu, Kyoto, Japan) as the detector. The chromatograms were recorded for the ultraviolet absorption of 254 nm. The system was calibrated using polystyrene standards. Weight-average molecular weight (M_w) was normalized to its starting weight, where the polydispersity index was calculated by dividing the M_w over number-average molecular weight.

STATISTICAL ANALYSIS. All datasets were tested for normality using the Shapiro-Wilk test, which confirmed a non-normal distribution of the data due to the limited sample size. Therefore, nonparametric tests were used for statistical analysis. All data were analyzed using a multiple comparison Kruskal-Wallis test and corrected by a Dunn's post-hoc test. Data are expressed as mean ± SD. Statistical differences were determined using Prism version 5.04 (GraphPad Software, La Jolla, California), and p values <0.05 were considered to indicate statistical significance.

For statistical analysis of the secant moduli, the native aorta and the bare graft were evaluated using a nonparametric Mann-Whitney *U* test, whereas the grafted aorta at different time points was evaluated using a nonparametric Kruskal-Wallis test followed by a Tukey-Kramer post-test. A p value <0.05 was considered to indicate statistical significance. Statistical analyses were performed using MATLAB and Statistics Toolbox Release 2012b (The MathWorks, Natick, Massachusetts).

RESULTS

MINIMALLY INVASIVE DELIVERY OF T-TEVGs. Balloon-expandable microfibrous T-TEVGs (n = 20) were made from biodegradable poly-L-lactic acid-based material, processed using electrospinning, and characterized using SEM with respect to inner diameter, wall thickness, and surface topology (Figures 1A to 1D). For in vitro evaluation, T-TEVGs (1.4 × 5 mm) were balloon-inflated to 2.0 mm, after which the inner diameter measured 2.09 ± 0.04 mm with a wall thickness of 138 ± 16 μm, and the luminal area measured 3.37 ± 0.15 mm^2. Surface topology after inflation exhibited a microporous morphology, to

FIGURE 3 Endothelium and Smooth Muscle Cells

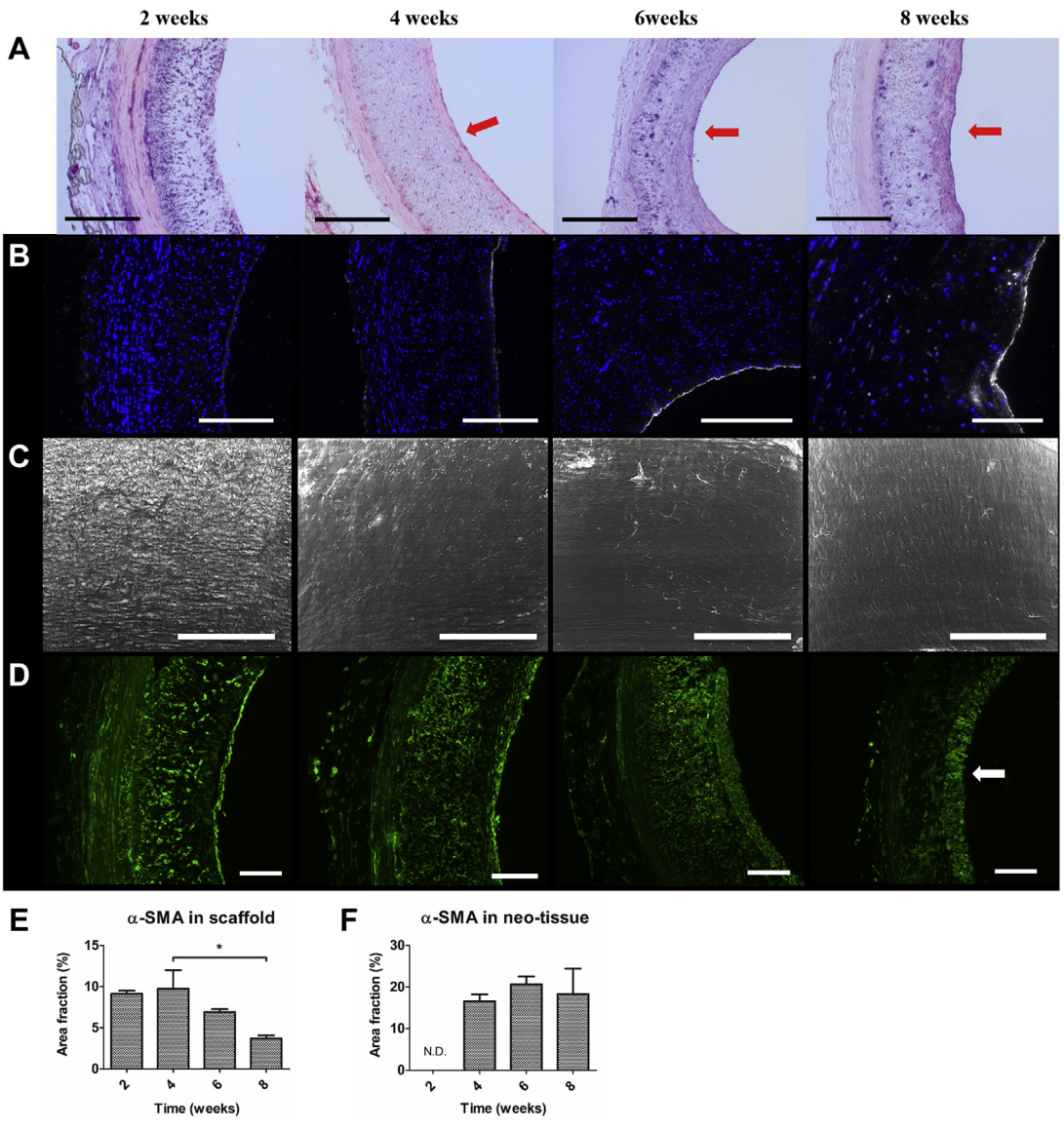

(A) Immunohistochemistry staining of CD31 for endothelial cells (indicated by the red arrows). Lumen is located at the right side of each picture. Scale bars represent 200 um. **(B)** Immunofluorescent costaining of von Willebrand factor for endothelium **(white)** and cell nuclei **(blue)**. Lumen is located at the right side of each picture. Scale bars represent 200 μm. **(C)** Scanning electron microscopic images of luminal side of transcatheter tissue-engineered vascular grafts (T-TEVGs). Scale bars represent 200 μm. **(D)** Immunofluorescent staining of alpha-smooth muscle actin (α-SMA) **(green)**. Lumen is located at the right side of each picture. Layer of α-SMA at 8-week explant indicated with **white arrow**. Scale bars represent 100 μm. **(E,F)** Area fraction (± SD) as a percentage of α-SMA in graft **(E)** and neotissue **(F)**. *$p < 0.05$. N.D. = not detected.

enable cellular infiltration into the T-TEVGs (Figure 1C) (35).

After graft characterization by SEM, a total of 20 animals underwent intervention, in which 19 T-TEVGs were successfully delivered and placed into the infrarenal abdominal aorta (Figures 1E to 1H) using a permissive minimally invasive procedure. One animal was excluded from the study during the implantation procedure because of an anomalous anatomy that made T-TEVG delivery not possible. The animal was subsequently sacrificed during the implantation procedure. Two animals were

FIGURE 4 Macrophage Presence

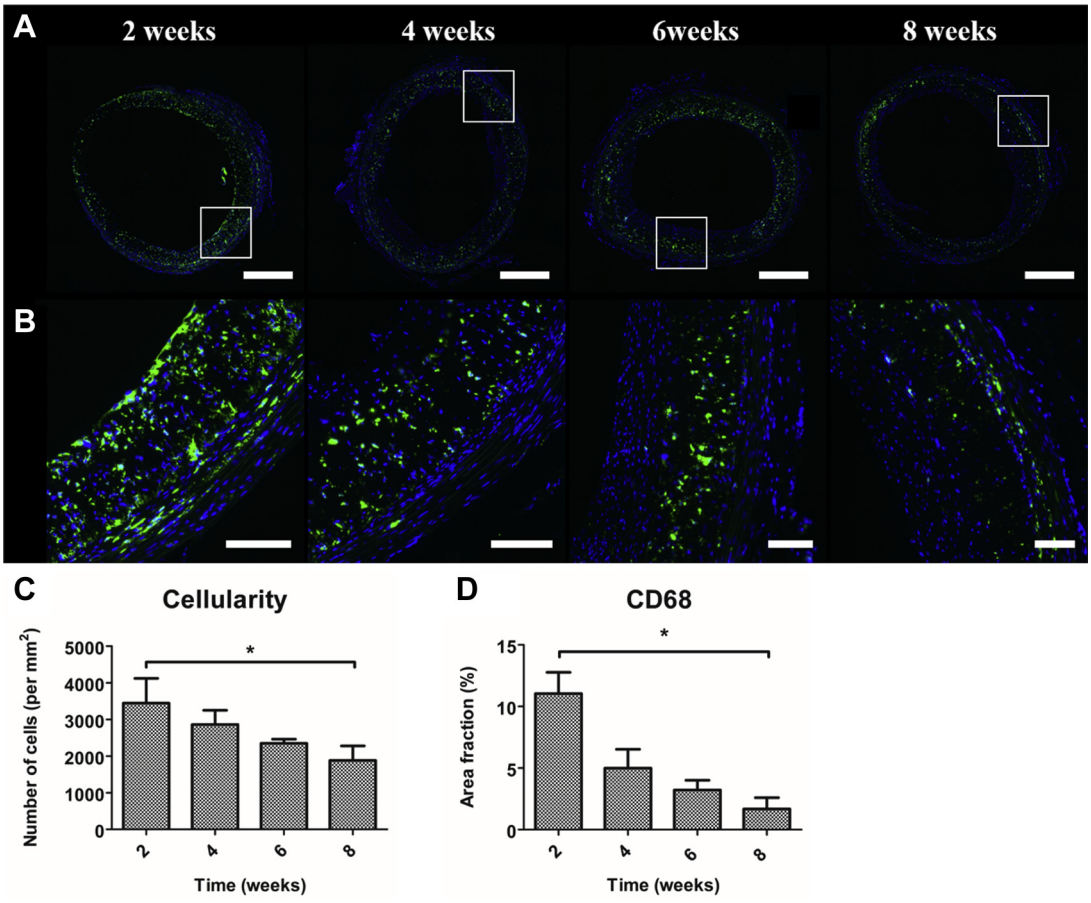

(A,B) Immunofluorescent costaining of CD68 (a pan-macrophage marker) **(green)** and cell nuclei **(blue)**. Scale bars represent 500 μm **(A)** and 100 μm **(B)**. **(C)** Cellularity (± SD) in number of cells per square millimeter. **(D)** Area fraction (± SD) as a percentage of CD68. *$p < 0.05$.

excluded because of post-operative complications; 1 animal died of bleeding immediately after surgery, probably caused by coagulation problems, and the other animal was euthanized because of lower limb paralysis from immediate graft thrombosis within 24 h. From the 17 animals that survived the implantation procedure, all T-TEVGs remained patent without showing clinical signs of graft failure throughout the duration of the study. Grafts were explanted after 1 day (n = 1), 2 weeks (n = 4), 4 weeks (n = 4), 6 weeks (n = 4), and 8 weeks (n = 4). No anticoagulants were used throughout the duration of the study.

GRAFT PATENCY AND EARLY TISSUE FORMATION IN ALL. T-TEVGs were defined as patent if more than 50% of the initial luminal surface area was maintained. Patency of grafts was confirmed by histological analyses of explants (Figures 2A and 2B). T-TEVGs did not show significant intimal hyperplasia with a stable midgraft luminal area over time (Figure 2C). Overall, wall thickness measured from histologic images remained constant over time (Figure 2D). The neointimal tissue that was formed on the luminal side consisted mainly of glycosaminoglycans after 4 weeks of implantation, as evident from Russell-Movat Pentachrome staining (Figures 2A and 2B). At later time points, T-TEVGs contained limited neointimal tissue consisting mainly of collagen (Figures 2A and 2B).

FULL ENDOTHELIAL CELL COVERAGE AND A GRADUAL TREND IN α-SMA-POSITIVE CELL MIGRATION TOWARD THE LUMINAL SIDE. Endothelial coverage of the graft is requested for optimal physiological function, to limit direct contact between blood and graft material, and to prevent thrombotic events. Over time, progressive endothelial coverage

FIGURE 5 Collagen Types I and III

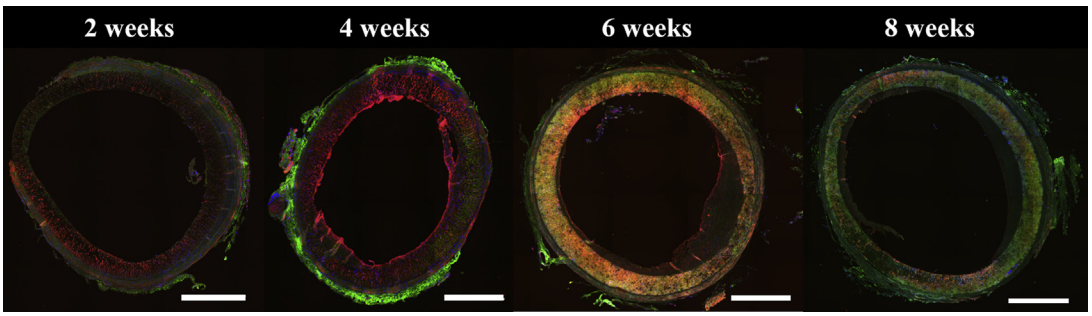

Immunofluorescent costaining of collagen type I **(green)**, collagen type III **(red)**, and cell nuclei **(blue)**. Scale bars represent 500 μm.

of the T-TEVGs was evident from both CD31 as well as von Willebrand factor (**Figures 3A and 3B**), which was in line with morphological observations from scanning electron microscopic analyses of the luminal surface (**Figure 3C**). Up to 2 weeks, bare graft could still be observed on the luminal side. After 4 weeks, however, advanced endothelial cell coverage of the luminal surface of T-TEVGs was seen, which ultimately developed into a confluent endothelial layer between 6 and 8 weeks (**Figure 3C**).

Additionally, α-SMA-positive cells are known for their tissue producing capacity, for which their presence is essential to induce neotissue formation (36,37). The distribution of α-SMA-positive cells, which could be either smooth muscle cells (SMCs) or myofibroblasts, clearly changed in time. At 4 and 6 weeks, α-SMA expression was detected mainly within the T-TEVG (**Figures 3D to 3F**). After 8 weeks, a layer of α-SMA-positive cells aligning on the luminal side of the graft could be observed, as indicated by the white arrow (**Figures 3D to 3F**).

DECREASE IN MACROPHAGE PRESENCE. Macrophages are known for steering tissue regeneration through their immune-modulating capacity, where a prolonged presence is indicative of an undesired chronic inflammatory response (20). Macrophage infiltration was evaluated on the basis of CD68 expression, a pan-macrophage marker. By 2 weeks, macrophage infiltration was observed inside the graft with an equal distribution over its thickness and local distribution by 8 weeks (**Figure 4A**). Over time, a significant decrease in both overall cellularity (3,445.362 ± 549.965 to 1,881.731 ± 321.848 cells; $p = 0.034$) as well as macrophages (11.040 ± 1.407 to 1.687 ± 0.736 area fraction (%); $p = 0.023$) was observed between 2 and 8 weeks (**Figures 4C and 4D**). As macrophages were present mainly in areas of polymer, their decline in number could indicate polymer resorption. Furthermore, a number of macrophages present at 8 weeks expressed arginase, an anti-inflammatory macrophage marker, suggesting that these macrophages promote functional tissue formation (Supplemental Figure S3) (20).

EARLY COLLAGEN TYPE III AND LATER STAGE COLLAGEN TYPE I FORMATION. Corresponding to cell colonization, considerable remodeling of the T-TEVG was seen at tissue level (**Figure 2**). To investigate one of the main important ECM components, we assessed expression of collagen types I and III, which are the most prevalent types of collagen in native blood vessels. By 2 weeks, early indications of collagen type III formation were observed in the grafts, even more predominant by 4 weeks, as indicated in **Figure 5**. By 6 weeks, early formation of collagen type I was seen, with colocalization of collagen types III and I. By 8 weeks, some grafts were observed to present predominantly type I inside the graft. This gradual transition from type III to type I over time might be indicative of collagen maturation.

ABUNDANT ENDOLUMINAL ELASTIN FORMATION. Elastin is a crucial ECM component required for vasomotion and is believed to have the capacity to inhibit neointima formation, which could lead to restenosis (38). In the explants, the native elastic layer can be observed at all time points (**Figures 6A and 6B**). However, by 4 weeks, a second elastic layer was observed on the luminal side of the graft, increasing in thickness at 6 weeks and covering the entire endoluminal space by 8 weeks. The results were confirmed by Elastica von Gieson staining (**Figure 6C**), clearly showing the elastic fibers in black by 8 weeks, highlighted by the red arrows (**Figure 6C**), showing similarity to the native internal thoracic artery (39).

JACC: BASIC TO TRANSLATIONAL SCIENCE VOL. 5, NO. 11, 2020
NOVEMBER 2020:1095–110

FIGURE 6 Elastin

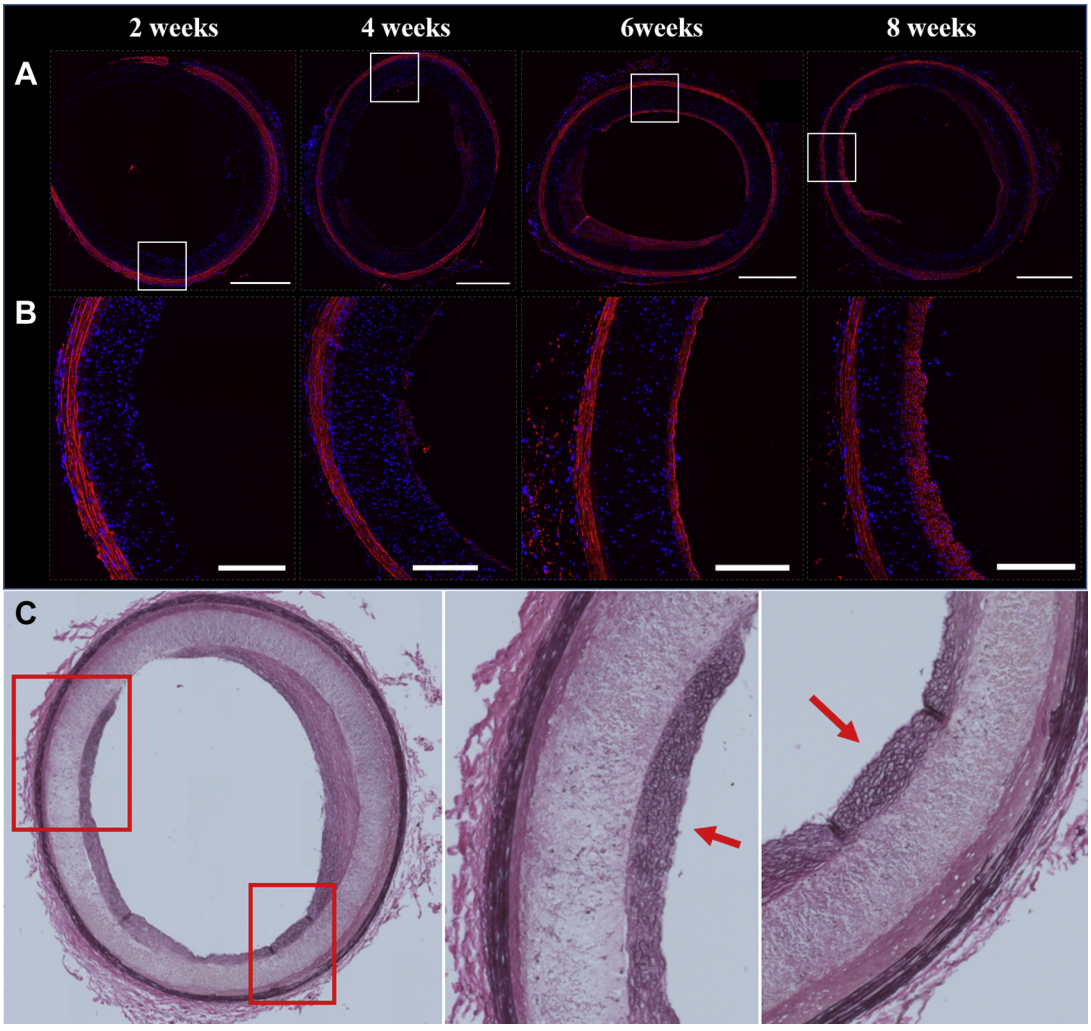

(A,B) Immunofluorescent costaining of elastin **(red)** and cell nuclei **(blue)**. Scale bars represent 500 μm **(A)** and 200 μm **(B)**. **(C)** Elastica von Gieson staining of an 8-week explant with close-up sections indicating elastic fibers in **black** as depicted by the **red arrows**.

MECHANICAL PROPERTIES OF T-TEVGs. Mechanical properties were assessed using uniaxial ring tensile tests. The differences in mechanical properties between native aorta and T-TEVG are illustrated in Figure 7A, in which the stress-strain curves and the low- and high-strain moduli were averaged and plotted as mean ± SD. The bare T-TEVG was stiffer than the native tissue, verified by a statistically significant difference of the secant modulus at low ($p = 0.029$) as well as high ($p = 0.029$) strains (Figure 7A).

The evolution of mechanical properties over time was divided into 2 periods: from implantation until week 4 and from week 4 until week 8. The first period is shown in Figure 7B, in which a decrease in stiffness is seen for high strain values. The stiffness decrease was significant between weeks 2 and 4 ($p = 0.050$). The second period is shown in Figure 7C, in which an increase in stiffness was evidenced for high strain values. The stiffness increase became significant ($p = 0.020$) between weeks 4 and 8. The low-strain moduli were found to be not significantly different in both periods.

DEGRADATION OF SCAFFOLDS. The aim of the graft is to degrade over time, when sufficient neotissue has been formed to take over the mechanical load. To characterize the remaining polymer over time, explanted T-TEVG s were analyzed using GPC.

FIGURE 7 Engineering Stress Versus Strain Curves and Secant Moduli

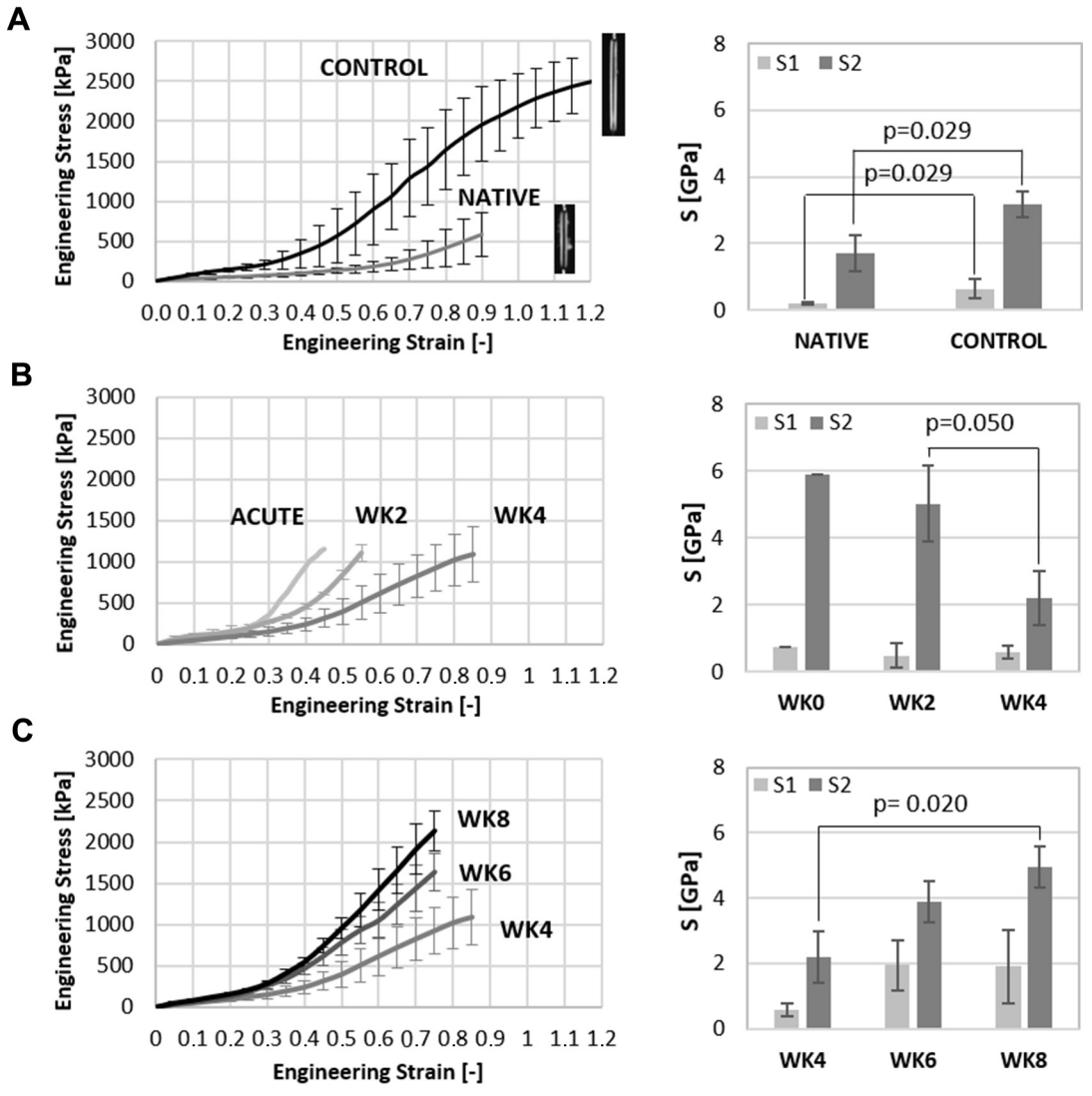

(A) Control (graft prior to implantation) and native samples. **(B)** acute (24-h), 2-week, and 4-week samples. **(C)** Four-week, 6-week, and 8-week samples. *S1* = low-strain modulus; *S2* = high-strain modulus.

After 4 weeks, the normalized M_w had declined to 93% and further decreased to 51% by 8 weeks (**Figure 8A**). The polydispersity index further showed a stable value of 1.3 up to 4 weeks and revealed elevated values of 2.5 and 2.7 by 6 and 8 weeks, respectively (**Figure 8B**), indicating polymer chain degradation.

ABSENCE OF CALCIFICATION. Explants were evaluated for adverse remodeling (e.g. calcifications) using Alizarin Red and von Kossa staining. Alizarin Red staining was absent in all explants (data not shown), whereas only 1 graft stained positive for 1 small and locally defined calcific event indicated by von Kossa staining (Supplemental Figure S4) at 6 weeks.

DISCUSSION

Here, we provide proof of concept of the transcatheter delivery and implantation of a novel regenerative T-TEVG that can be successfully delivered and

FIGURE 8 Degradation Analyzed Using Gel Permeation Chromatography

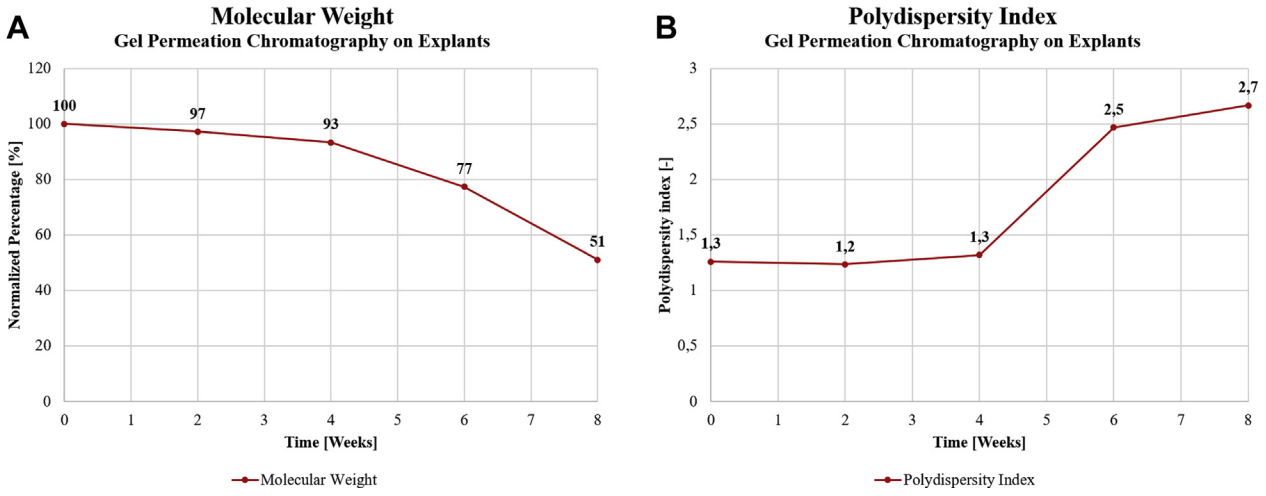

(A) Molecular weight. **(B)** Polydispersity index.

deployed into the artery and induce regeneration. This study demonstrates maintenance of graft patency for up to 2 months with full endothelial coverage between 6 and 8 weeks and the formation of native tissue components such as collagen types I and III by 8 weeks. Most strikingly, we observed abundant elastin formation, covering the entire endoluminal side of the graft, strongly suggesting the regenerative potential of the device. Furthermore, a decrease in the molecular weight of the graft was seen, while the mechanical properties further evolved over time. This study is the first to describe the possibility to regenerate an artery using a minimally invasive approach, by implanting a fully synthetic and off-the-shelf graft. Inspired by in situ TE and stent technologies, we combined 2 advanced manufacturing fields to develop a biodegradable regenerative T-TEVG with the capacity to expand and exert forces on the native artery.

In contrast to existing bioresorbable vascular scaffolds (BVS) used for stenting application, the bioresorbable T-TEVG presented here is distinguished by the microstructure that is optimized for regeneration. One of the main limitations of current BVS design is the necessity of large struts to meet the required radial strength of their metallic counterparts (40). As a consequence, the larger luminal protrusion of struts disrupts laminar blood flow, resulting in disturbed flow and the associated low and reciprocating endothelial shear stress, which subsequently could promote platelet activation (41,42). Recent findings from the AIDA trial as well as the ABSORB II trial indicate that BVS are associated with a higher rate of device thrombosis than drug-eluting metallic stents (29,30). The causes for this could partially be attributed to disturbances in blood flow, direct exposure to the damaged vascular wall, stent malapposition, long-term stent resorption, and incomplete (endothelial) coverage of the stent itself. To maintain laminar flow, a different approach in design is warranted. Through the absence of big struts, the T-TEVG could minimize regions of disturbed flow. In addition, its porous microstructure not only provides a template to host cells for tissue regeneration but also offers a bigger contact area between polymer and cells responsible for biodegradation, thereby reducing resorption time.

One of the objectives in vascular TE is to enhance the endothelialization of grafts due to their modulating function in vascular biology, thereby maintaining homeostasis (43-45). The establishment of an endothelial layer in grafts is considered of great importance to prevent complications such as reduced patency due to thrombosis or intimal hyperplasia (45). In this study, rapid endothelial coverage of T-TEVGs was observed, which led to a fully confluent endothelial layer at week 8. This is consistent with several other studies that showed rapid endothelialization of grafts (31,32,46,47). The rapid endothelialization of our grafts may have contributed to the absence of thrombotic events, although animals were deprived of antiplatelet therapy throughout the study.

α-SMA-positive cells are crucial for tissue formation, as they have the capacity to synthesize glycosaminoglycans, collagen, and elastin (36,37). This makes this cell type of particular interest for the regenerative potential of the graft. We observed that the distribution of α-SMA-positive cells varied over time during the study. Until week 4, α-SMA expression was detected mainly within the T-TEVG, whereas at later time points, α-SMA was expressed predominantly on the luminal side. This can be explained by the plastic phenotype nature of this cell type, ranging from quiescent and contractile to proliferative and synthetic, with intermediate phenotypes in between (36). As SMCs can shift their phenotype reversibly, harnessing their plasticity is an important target for vascular TE. Proliferation of synthetic SMCs allows ECM formation and remodeling, which is required to provide the T-TEVG with sufficient mechanical strength. However, returning SMCs to a quiescent and contractile phenotype is warranted to avoid adverse remodeling that can lead to intimal hyperplasia, an important determinant of long-term graft failure.

In this study, α-SMA-positive cells were observed mainly inside the graft by 4 and 6 weeks, which aligns with the observation of increased collagen type III formation. Furthermore, their gradual migration toward the luminal side and colocalization with the elastin formation suggests that these cells were also responsible for elastin formation. A possible explanation for the gradual decrease in α-SMA expression inside the graft may be found in the observed stiffening of the T-TEVGs, which may have led to reduced cyclic strains of the residing cells, reversing its expression back to a quiescent state. On the contrary, the prolonged α-SMA expression on the luminal side might be explained by its exposure to cyclic strains of the bloodstream, as it is known that mechanical cues can trigger α-SMA expression (36,48).

The synthetic T-TEVG clearly triggered endogenous neotissue formation within, which demonstrated an increasingly mature organization of ECM components, with remarkable abundant presence of elastic fibers on the luminal surface of the graft. After 8 weeks in vivo, multilayered elastic fibers were present, showing good resemblance to the internal thoracic artery, which is the golden standard in current clinical bypass treatment (39). Essential for long-term functioning of the neoartery is the presence of a mature elastic network, which has been so far a major challenge in vascular TE (49). The formation of elastin in our T-TEVGs is therefore of pivotal importance and indicates the advanced maturation and functionality of our grafts.

Crucial for our in situ approach is the timely resorption of graft material during the regeneration of an autologous artery to avoid adverse remodeling (40,50). After 8 weeks, we observed ongoing graft resorption, with most graft material still present and most essential tissue components in place.

In this study we analyzed the mechanical properties of a minimally invasive bioabsorbable graft with regeneration capacity, the bare native aorta, and the scaffolded aorta over time. Considerable discrepancies were found when comparing the stiffness of the graft and the native aorta at low and high strains, confirming its capacity to provide structural support to the artery. Nevertheless, once the T-TEVG had been implanted, all grafted aortas presented similar low strain stiffness over time. This can be explained by the fact that all follow-up explants include the graft as well as the native tissue and that possible changes, motivated by graft degradation on tissue formation, are not noticeable when the stretch is low. In contrast, at high strains, a clear softening effect is experienced during the first weeks in the grafted aorta, followed by a subsequent stiffening over time. This could suggest that early degradation of the graft motivates a drop of mechanical properties, nonetheless further degradation is compensated by tissue buildup. As considerable scaffold remnants are still present within the neotissue by week 8, longer term follow-up would be required to evaluate the evolution of mechanical properties at high strains as the implant's resorption evolves. Nevertheless, we expect no further changes in stiffness once the implant has fully resorbed.

Given the T-TEVG's features of combining transcatheter delivery, mechanical support, and regenerative capacity, we envision future potential application in atherosclerotic and aneurysmatic arterial indications, in which instant opening and/or mechanical reinforcement of the arterial wall is required, followed by long-term tissue restoration to ensure long-term functionality. Moreover, the regenerative capacity of the T-TEVG could allow growth when applied in pediatric patients with congenital defects. Our approach of using synthetic vascular grafts made of a U.S. Food and Drug Administration-approved biodegradable polymer-based material makes it clinically appealing because of its off-the-shelf availability. In contrast to grafts that are composed of cellular content, it does not involve limited storage issues or specialized cryopreservation techniques (51). Furthermore, it does not require costly and time-consuming laboratory techniques used to engineer vessels in vitro, whether

JACC: BASIC TO TRANSLATIONAL SCIENCE VOL. 5, NO. 11, 2020
NOVEMBER 2020:1095–110

or not followed by decellularization (10,11,14). Processing the material by electrospinning further allows optimal control over the porosity and mechanical properties through precise fiber organization (35,52).

STUDY LIMITATIONS. First, T-TEVGs were implanted in healthy animals, without atherosclerotic or aneurysmatic burden. Because of the dimensions of the animal's vasculature, we were forced to adjust our implantation technique. Instead of performing a completely minimally invasive procedure, in which a catheter is inserted through the femoral or radial artery, we performed a median laparotomy to obtain full exposure of the target vessel (rat abdominal aorta). When full exposure of the vessel was obtained, we performed a permissive minimally invasive procedure in which the T-TEVG mounted on the balloon catheter was inserted and deployed under surgical view. Temporal noninvasive imaging analysis during the study would be of great additional value to monitor in vivo functionality of T-TEVGs after implantation. This would probably require labeling of the T-TEVG to distinguish it from the surrounding tissues. Nevertheless, the main objectives of this proof-of-concept study were to demonstrate the capacity of our novel T-TEVG to be minimally invasively delivered and to induce regeneration by the host. Future studies will be performed in larger, translational animal models, which will allow complete minimally invasive delivery of T-TEVGs in clinically relevant vascular regions. This should shed more light on the regenerative capacity of these grafts in further translation to human applications. These studies will include temporal assessment of in vivo functionality by different imaging modalities and longer follow-up times.

CONCLUSIONS

This proof-of-concept study shows the first successful minimally invasive delivery of a novel regenerative T-TEVG with full patency for up to 2 months, extensive cellular infiltration with subsequent rapid endothelialization, and favorable matrix production and remodeling with abundant neoendoluminal elastin formation. These promising short-term results in a small animal model hold future potential for various clinical indications in a variety of patients with cardiovascular disease.

ACKNOWLEDGMENTS The authors thank Dr. Serena Buscone and Arturo Lichauco, MSc, (Department of Biomedical Engineering, Eindhoven University of Technology) for assistance and expert advice on histology, and Prof. Dr. Patricia Dankers for critical analysis of the manuscript.

AUTHOR DISCLOSURES

This work was funded by a grant from the Dutch government to the Netherlands Institute for Regenerative Medicine (grant FES0908). The authors gratefully acknowledge funding from the Ministry of Education, Culture and Science for the Gravitation Program 024.003.103 "Materials Driven Regeneration." Stentit provided funding to this study through a soft loan provided by the Dutch government (STW Take-Off Phase 2, project 15672). Drs. Bart Sanders and Maria Cabrera are founders and shareholders of Stentit B.V. Drs. Bart Sanders, Maria S. Cabrera, and Frank P.T. Baaijens are the holders of a patent related to the presented graft technology. All other authors have reported that they have no relationships relevant to the contents of this paper to disclose.

ADDRESS FOR CORRESPONDENCE: Dr. Carlijn V.C. Bouten, Eindhoven University of Technology, Department of Biomedical Engineering, PO Box 513, 5600 MB Eindhoven, the Netherlands. E-mail: c.v.c.bouten@tue.nl.

PERSPECTIVES

COMPETENCY IN MEDICAL KNOWLEDGE: Given the benefits of combining transcatheter delivery, mechanical support, and regenerative capacity in 1 biodegradable "device," we envision future potential application in atherosclerotic and aneurysmatic arterial indications, in which instant opening and/or mechanical reinforcement of the arterial wall is required, followed by long-term tissue restoration to ensure long-term functionality. In particular, this small diameter balloon expandable device might be used for below-the-knee or coronary indications. Here, restoration of the endoluminal elastin layer in combination with its full degradable capacity, could prevent long-term restenosis. The degradability and regenerative capacity of the device allow tissue growth when applied in pediatric patients with congenital defects (e.g., coarctation of the aorta).

TRANSLATIONAL OUTLOOK: The outcome accomplished in this proof-of-concept study in a small animal model warrants future studies in larger animal models, which allow testing in more challenging conditions in clinical relevant vascular regions for longer periods to evaluate the long-term outcomes.

REFERENCES

1. Chlupáč J, Filová E, Bačáková L. Blood vessel replacement: 50 years of development and tissue engineering paradigms in vascular surgery. Physiol Res 2009;58:S119–39.

2. Sabik JF, Lytle BW, Blackstone EH, Houghtaling PL, Cosgrove DM. Comparison of saphenous vein and internal thoracic artery graft patency by coronary system. Ann Thorac Surg 2005;79:544–51.

3. Klinkert P, Post PN, Breslau PJ, van Bockel JH. Saphenous vein versus PTFE for above-knee femoropopliteal bypass. A review of the literature. Eur J Vasc Endovasc Surg 2004; 27:357–62.

4. Pashneh-Tala S, MacNeil S, Claeyssens F. The tissue-engineered vascular graft—past, present, and future. Tissue Eng Part B Rev 2016;22: 68–100.

5. Isenberg BC, Williams C, Tranquillo RT. Small-diameter artificial arteries engineered in vitro. Circ Res 2006;98:25–35.

6. Chard RB, Johnson DC, Nunn GR, Cartmill TB. Aorta-coronary bypass grafting with polytetrafluoroethylene conduits. Early and late outcome in eight patients. J Thorac Cardiovasc Surg 1987;94: 132–4.

7. Collins P, Webb CM, Chong CF, Moat NE. for the Radial Artery Versus Saphenous Vein Patency (RSVP) Trial Investigators. Radial artery versus saphenous vein patency randomized trial: Five-year angiographic follow-up. Circulation 2008;117:2859–64.

8. Haruguchi H, Tereoka S. Intimal hyperplasia and haemodynamic factors in arterial bypass and arteriovenous grafts: a review. J Artif Organs 2003;6:227–35.

9. L'Heureux N, Paquet S, Labbe R, Germain L, Auger FA. A completely biological tissue-engineered human blood vessel. FASEB J 1998; 12:47–56.

10. McAllister TN, Maruszewski M, Garrido SA, et al. Effectiveness of haemodialysis access with an autologous tissue-engineered vascular graft: a multicenter cohort study. Lancet 2009;373: 1440–6.

11. Wystrychowski W, McAllister TN, Zagalski K, Dusserre N, Cierpka L, L'Heureux N. First human use of an allogenic tissue-engineered vascular graft for hemodialysis access. J Vasc Surg 2014; 60:1353–7.

12. Niklason LE, Gao J, Abbott WM, et al. Functional arteries grown in vitro. Science 1999;284: 489–93.

13. Gui L, Boyle MJ, Kamin YM, et al. Construction of tissue-engineered small-diameter vascular grafts in fibrin scaffolds in 30 days. Tissue Eng Part A 2014;20:1499–507.

14. Lawson JH, Glickman MH, Ilzecki M, et al. Bioengineered human acellular vessels for dialysis access in patient with end-stage renal disease: two phase 2 single-arm trials. Lancet 2016;387: 2026–34.

15. Shin'oka T, Imai Y, Ikada Y. Transplantation of a tissue-engineered pulmonary artery. N Engl J Med 2001;344:532–5.

16. Shin'oka T, Matsumura G, Hibino N, et al. Midterm clinical result of tissue-engineered vascular autografts seeded with autologous bone marrow cells. J Thorac Cardiovasc Surg 2005;129: 1330–8.

17. Hibino N, McGillicuddy E, Matsumura G, et al. Late-term results of tissue-engineered vascular grafts in humans. J Thorac Cardiovasc Surg 2010; 139:431–6.

18. Bockeria LA, Svanidze O, Kim A, et al. Total cavopulmonary connection with a new bioabsorbable vascular graft: first clinical experience. J Thorac Cardiovasc Surg 2017;153:1542–50.

19. Roh JD, Sawh-Martinez R, Brennan MP, et al. Tissue-engineered vascular grafts transform into mature blood vessels via an inflammation-mediated process of vascular remodeling. Proc Natl Acad Sci U S A 2010;107:4669–74.

20. Wissing TB, Bonito V, Bouten CVC, Smits AIPM. Biomaterial-driven in situ cardiovascular tissue engineering—a multi-disciplinary perspective. NPJ Regen Med 2017;2:18.

21. Tara S, Kurobe H, Maxfield MW, et al. Evaluation of remodeling process in small-diameter cell-free tissue-engineered arterial graft. J Vasc Surg 2015;62:734–43.

22. Serruys PW, Chevalier B, Dudek D, et al. A bioresorbable everolimus-eluting scaffold versus a metallic everolimus-eluting stent for ischaemic heart disease caused by de-novo native coronary artery lesions (ABSORB II): an interim 1-year analysis of clinical and procedural secondary outcomes from a randomised controlled trial. Lancet 2015;385:43–54.

23. Puricel S, Arroyo D, Corpataux N, et al. Comparison of everolimus and biolimus-eluting coronary stents with everolimus-eluting bioresorbable vascular scaffolds. J Am Coll Cardiol 2015;65: 791–801.

24. Ellis SG, Kereiakes DJ, Metzger DC, et al. Everolimus-eluting bioresorbable scaffolds for coronary artery disease. N Engl J Med 2015;373: 1905–15.

25. Gao R, Yang Y, Han Y, et al. Bioresorbable vascular scaffolds versus metallic stents in patients with coronary artery disease: ABSORB China trial. J Am Coll Cardiol 2015;66:2298–309.

26. Kimura T, Kozuma K, Tanabe K, et al. A randomized trial evaluating everolimus-eluting Absorb bioresorbable scaffolds vs. everolimus-eluting metallic stents in patients with coronary artery disease: ABSORB Japan. Eur Heart J 2015; 36:3332–42.

27. Sabate M, Windecker S, Iniguez A, et al. Everolimus-eluting bioresorbable stent vs. durable polymer everolimus-eluting metallic stent in patients with ST-segment elevation myocardial infarction: results of the randomized ABSORB ST-segment elevation myocardial infarction-TROFI II trial. Eur Heart J 2016;37:229–40.

28. Onuma Y, Sotomi Y, Shiomi H, et al. Two-year clinical, angiographic, and serial optical coherence tomographic follow-up after implantation of an everolimus- eluting bioresorbable scaffold and an everolimus-eluting metallic stent: insights from the randomised ABSORB Japan trial. EuroIntervention 2016;12:1090–101.

29. Serruys PW, Chevalier B, Sotomi Y, et al. Comparison of an everolimus-eluting bioresorbable scaffold with an everolimus-eluting metallic stent for the treatment of coronary artery stenosis (ABSORB II): a 3 year, randomised, controlled, singleblind, multicentre clinical trial. Lancet 2016;388:2479–91.

30. Wykrzykowska JJ, Kraak RP, Hofma SH, et al. Bioresorbable scaffolds versus metallic stents in routine PCI. N Engl J Med 2017;376:2319–28.

31. Duijvelshoff R, van Engeland NCA, Gabriels KMR, et al. Host response and neo-tissue development during resorption of a fast-degrading supramolecular electrospun arterial scaffold. Bioengineering (Basel) 2018;5:E61.

32. Talacua H, Smits AIPM, Muylaert DEP, et al. In situ tissue engineering of functional small-diameter blood vessels by host circulating cells only. Tissue Eng Part A 2015;21:2583–94.

33. Sheehan DC, Hrapchak BB. Theory and Practice of Histotechnology. 2nd ed. St. Louis, Missouri: Mosby, 1980.

34. van Haaften EE, van Turnhout MC, Kurniawan NA. Image-based analysis of uniaxial ring test for mechanical characterization of soft materials and biological tissues. Soft Matter 2019; 15:3353–61.

35. Balguid A, Mol A, van Marion MH, Bank RA, Bouten CV, Baaijens FP. Tailoring fiber diameter in electrospun poly(epsilon-caprolactone) scaffolds for optimal cellular infiltration in cardiovascular tissue engineering. Tissue Eng Part A 2009;15: 437–44.

36. Rensen SSM, Doevendans PAFM, van Eys GJJM. Regulation and characteristics of vascular smooth muscle cell phenotypic diversity. Neth Heart J 2007;15:100–8.

37. Beamish JA, He P, Kottke-Marchant K, Marchant RE. Molecular regulation of contractile smooth muscle cell phenotype: implications for vascular tissue engineering. Tissue Eng Part B Rev 2010;16:467–91.

38. Sugiura T, Agarwal R, Tara S, et al. Tropoelastin inhibits intimal hyperplasia of mouse bioresorbable arterial vascular grafts. Acta Biomater 2017;52:74–80.

39. Kinoshita T, Asai T, Suzuki T, Van Phung D. Histomorphology of right versus left internal thoracic artery and risk factors for intimal hyperplasia. Eur J Cardiothorac Surg 2014;45: 726–31.

40. Indolfi C, De Rosa S, Colombo A. Bioresorbable vascular scaffolds—basic concepts and clinical outcome. Nat Rev Cardiol 2016;13: 719–29.

41. Chiu J-J, Chien S. Effects of disturbed flow on vascular endothelium: pathophysiological basis and clinical perspectives. Physiol Rev 2011;91:10–1152.

42. Bourantas CV, Papafaklis MI, Kotsia A, et al. Effect of the endothelial shear stress patterns on neointimal proliferation following drug-eluting bioresorbable vascular scaffold implantation: an optical coherence tomography study. J Am Coll Cardiol Intv 2014;7:315–24.

43. Rubanyi GM. The role of endothelium in cardiovascular homeostasis and diseases. J Cardiovasc Pharmacol 1993;22:S1–14.

44. Pearson JD. Endothelial cell function and thrombosis. Best Pract Res Clin Haematol 1999;12:329–41.

45. Patel SD, Waltham M, Wadoodi A, Burnand KG, Smith A. The role of endothelial cells and their progenitors in intimal hyperplasia. Ther Adv Cardiovasc Dis 2010;4:129–41.

46. Wu W, Allen RA, Wang Y. Fast-degrading elastomer enables rapid remodeling of a cell-free synthetic graft into a neo-artery. Nat Med 2012;18:1148–53.

47. Quint C, Arief M, Muto A, Dardik A, Niklason LE. Allogeneic human tissue-engineered blood vessel. J Vasc Surg 2012;55:790–8.

48. Bono N, Pezzoli D, Levesque L, et al. Unraveling the role of mechanical stimulation on smooth muscle cells: a comparative study between 2D and 3D models. Biotechnol Bioeng 2016;113:2254–63.

49. Patel A, Fine B, Sandig M, Mequanint K. Elastin biosynthesis: the missing link in tissue-engineered blood vessels. Cardiovasc Res 2006;71:40–9.

50. de Valence S, Tille JC, Mugnai D, et al. Long term performance of polycaprolactone vascular grafts in a rat abdominal aorta replacement model. Biomaterials 2012;33:38–47.

51. Pascual G, García-Honduvilla N, Rodríguez M, Turégano F, Bujan J, Bellón JM. Effect of the thawing process on cryopreserved arteries. Ann Vasc Surg 2001;15:619–27.

52. Soliman S, Sant S, Nichol JW, Khabiry M, Traversa E, Khademhosseini A. Controlling the porosity of fibrous scaffolds by modulating the fiber diameter and packing density. J Biomed Mater Res Part A 2011;96:566–74.

KEY WORDS elastin, regeneration, tissue engineering, transcatheter delivery, vascular graft

APPENDIX For supplemental figures and a table, please see the online version of this paper.